ISSN 0036-0236, Russian Journal of Inorganic Chemistry, 2018, Vol. 63, No. 1, pp. 116–120. © Pleiades Publishing, Ltd., 2018.

PHYSICOCHEMICAL ANALYSIS OF INORGANIC SYSTEMS

Solubilities, Densities, and Refractive Indices in the Quaternary System ($Li_2B_4O_7$ + $Na_2B_4O_7$ + $Mg_2B_6O_{11}$ + H_2O) at 298.15 K[1]

Shi-Qiang Wang[a, b, *], Yun Song[a], Xue-Min Du[a], Ya-Fei Guo[a, b], and Tian-Long Deng[a, b]

[a] *College of Chemical Engineering and Materials Science, Tianjin University of Science and Technology, Tianjin, 300457 P. R. China*

[b] *Tianjin Key Laboratory of Marine Resources and Chemistry, Tianjin, 300457 P. R. China*

**e-mail: wangshiqiang@tust.edu.cn*

Received July 8, 2016

Abstract—Solubilities, densities, and refractive indices in the quaternary system ($Li_2B_4O_7$ + $Na_2B_4O_7$ + $Mg_2B_6O_{11}$ + H_2O) at $T = 298.15$ K and $p = 0.1$ MPa were investigated experimentally with the method of isothermal dissolution equilibrium. According to the experimental data, the phase diagrams and the diagrams of densities and refractive indices versus lithium tetraborate composition in the solution were plotted, respectively. In the phase diagrams of the quaternary system at 298.15 K, there are one invariant point, three univariant isotherm dissolution curves, and three crystallization regions corresponding to $Li_2B_4O_7 \cdot 3H_2O$, $Na_2B_4O_7 \cdot 10H_2O$ and $Mg_2B_6O_{11} \cdot 15H_2O$, respectively. The size of crystallization areas of salt is in the order $Mg_2B_6O_{11} \cdot 15H_2O > Na_2B_4O_7 \cdot 10H_2O > Li_2B_4O_7 \cdot 3H_2O$, which demonstrates $Mg_2B_6O_{11} \cdot 15H_2O$ can be more easily separated from solution in this quaternary system. The solution density and refractive index of the quaternary system at 298.15 K change regularly with the increasing of $Li_2B_4O_7$ concentration. The calculated values of density and refractive index using empirical equations of the quaternary system are in good agreement with the experimental values.

DOI: 10.1134/S0036023618010175

INTRODUCTION

Boron plays important roles in many industries. Boron compounds are used extensively in the pigment, papermaking, medicine, and textile industries, etc. There are more than seven hundred salt lakes with an area larger than 1 km^2 in the Qinghai-Tibet Plateau. The Salt Lake of Qaidam Basin consists of a series of lakes including the Dong-Xi-Taijinaier Lake, Da-Xiao-Chaidan Lake, and Yiliping Lake, and is one of the subtypes of magnesium sulfate brines famous for its abundance of lithium, potassium, and boron resources [1–4]. The main components of its brines can be described with the $Li^+ + Na^+ + K^+ + Mg^{2+} + Cl^- + SO_4^{2-}$ + borate + H_2O system. It is well-known that phase diagrams and phase equilibria play an important role in exploiting brine resources and describing the geochemical behavior of brine mineral. To exploit the valuable brine resources economically, the phase equilibria and phase diagrams of brine systems containing boron at different temperatures are required.

Aiming at understanding the thermodynamic properties of boron-containing brine, some solid-liquid phase equilibria systems at different temperatures have been done by our research group [5–10]. However, the investigations on thermodynamic properties of the aqueous solutions containing borates are lack, this might be due to the variety of the present forms of polyborates, such as monoborate $[B(OH)_4^-]$, diborate $[B_2O(OH)_6^{2-}]$, triborate $[B_3O_3(OH)_5^-]$, and polytetraborate $[B_4O_5(OH)_4^{2-}$, $B_5O_6(OH)_4^-$, $B_6O_7(OH)_6^{2-}]$, and the dissolving behavior of boron is very complicated. In this paper, the isothermal solubilities and solution densities, refractive indices of the quaternary system ($Li_2B_4O_7$ + $Na_2B_4O_7$ + $Mg_2B_6O_{11}$ + H_2O) at 298.15 K were presented by the isothermal dissolution equilibrium method to describe the stable behaviors to separate and purify the borate-containing mixture salts.

EXPERIMENTAL

Apparatus and Reagents

A magnetic stirring thermostatic water bath (HXC-500-12A, Beijing Fortunejoy Sci. Technol. Co. Ltd.) was used to control the temperature with a precision of 0.01 K. The application of the polarizing microscope (BX51, Olympus Co., Japan) and X-ray powder diffractometer (MSAL XD-3, Beijing Purkinje Instru-

[1] The article is published in the original.

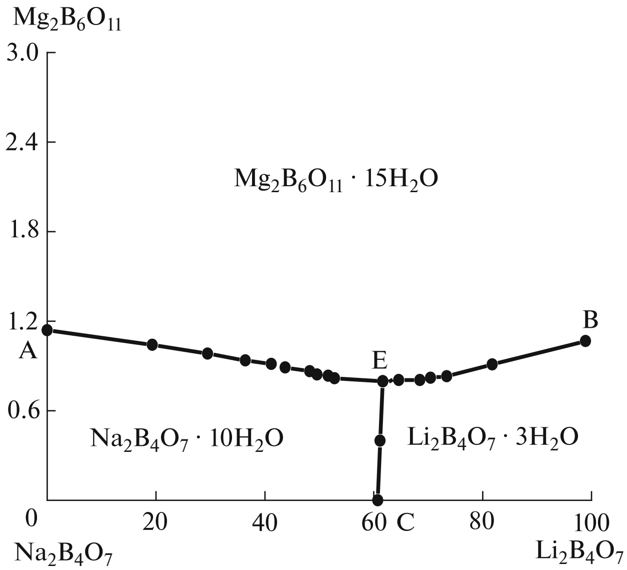

Fig. 1. Dry-salt phase diagram of the quaternary system ($Li_2B_4O_7 + Na_2B_4O_7 + Mg_2B_6O_{11} + H_2O$) at 298.15 K.

ment Co. Ltd., China) was to identify the crystal structures of solid phases. An inductively coupled plasma optical emission spectrometer (ICP-OES, Prodigy, Leman Co., USA) was employed to determine the concentrations of Li^+ in solution.

The chemicals of analytical grade were obtained from the Sinopharm Chemical Reagent Co., Ltd: lithium borate trihydrate ($Li_2B_4O_7 \cdot 3H_2O$, 0.992 in mass fraction), borax ($Na_2B_4O_7 \cdot 10H_2O$, 0.995 in mass fraction), and were re-crystallized with doubly deionized water (DDW) before use. Inderite ($Mg_2B_6O_{11} \cdot 15H_2O$, 0.99 in mass fraction) was synthesized in our laboratory with the method described in the literature [11]. Doubly deionized water (DDW) with conductivity less than 1×10^{-4} S m^{-1} was used to prepare the series of the artificial synthesized brines and chemical analysis.

Method

The isothermal dissolution method was used in this study, and more details of the experimental method are available in our previous works [12–14]. In briefly, the series of artificial synthesized complexes were sealed in hard polyethylene bottles and placed in the magnetic stirring thermostatic bath (HXC-500-6A). The temperatures of the baths were set at 298 ± 0.01 K with 150 rpm stirring speed in order to accelerate the establishment of equilibrium states. After these artificial synthesized complexes were stirred for about (3 to 5) days, it could be found that the equilibrium had been reached when the compositions of the liquid phase were determined and became constant state. Before taking sampling, it took about 1 h for the clarification of the aqueous solution. Two samples were taken out from the bottles. One was used for determining physicochemical properties including density and refractive index of the liquid phase of the quaternary system. The other was applied to quantitative analysis. In addition, the solid phase minerals were identified with X-ray powder diffraction.

The concentration of boron in liquid phase was analyzed by the weight methods of mannitol with sodium hydroxide standard solution in the presence of double indicator of methyl red and phenolphthalein, and the relative error of the analytical results is less than ±0.003 in mass fraction. The Mg^{2+} ion concentration was determined with modified EDTA complexometric titration method in the presence of Eriochrome Black-T as the indicator. The interference of the coexisted lithium ion in brine can be efficiently eliminated using butanol and anhydrous alcohol as a masking agent, and the uncertainty is less than ±0.003 in mass fraction [15]. The Li^+ concentration was evaluated with ICP-OES measurement.

The measurements of the liquid-phase physicochemical properties were corresponding to density and refractive index. The densities (ρ) were measured using a digital vibrating-tube densimeter (DMA 4500, Anton Paar Co. Ltd., Austria) with an uncertainty of ±0.00001 g cm^{-3}. An Abbe refractometer (WZS-1, Shanghai Yuguang Instrument Co. Ltd., China) was used to measure the refractive index (n_D) with an accuracy of ±0.0001. All the measurements were maintained at the desired temperature with ±0.01 K through control of the thermostat (K20-cc-NR, Huber, Germany).

RESULTS AND DISCUSSION

Phase Diagram of the Quaternary System ($Li_2B_4O_7 + Na_2B_4O_7 + Mg_2B_6O_{11} + H_2O$)

The experimental data on the solubilities, densities and refractive indices of the quaternary system ($Li_2B_4O_7 + Na_2B_4O_7 + Mg_2B_6O_{11} + H_2O$) at 298.15 K were determined and presented in Table 1. The composition of the liquid phase in the quaternary system was expressed in mass fraction and Jänecke index [J_b/(g/100 g dry salt)]. According to the experimental data in Table 1, the stable phase diagrams of the quaternary system at 298.15 K were plotted, as shown in Figs. 1 and 2.

In Fig. 1, the dry-salt phase diagram consists of three crystallization zones corresponding to lithium borate trihydrate ($Li_2B_4O_7 \cdot 3H_2O$), borax ($Na_2B_4O_7 \cdot 10H_2O$) and inderite ($Mg_2B_6O_{11} \cdot 15H_2O$), three univariant isothermal dissolution curves of AE, BE and CE, indicating the cosaturation of two salts. The size of crystallization areas of salt is in the order $Mg_2B_6O_{11} \cdot 15H_2O > Na_2B_4O_7 \cdot 10H_2O > Li_2B_4O_7 \cdot 3H_2O$, which demonstrates $Mg_2B_6O_{11} \cdot 15H_2O$ can be more easily separated from the solution in this quaternary system.

Table 1. Solubilities and physicochemical properties of the quaternary system ($Li_2B_4O_7$ + $Na_2B_4O_7$ + $Mg_2B_6O_{11}$ + H_2O) at 298.15 K

no.	Composition of liquid phase $w_i \times 10^2$				Jänecke index J_b/(g/100 g dry salt)			density ρ/(g cm^{-3})	n_D	Solid phase
	$Li_2B_4O_7$	$Na_2B_4O_7$	$Mg_2B_6O_{11}$	H_2O	$Li_2B_4O_7$	$Na_2B_4O_7$	H_2O			
1, A	0.00	2.95	0.034	97.02	0.00	98.86	3251.21	1.02465	1.3388	$Na_2B_4O_7 \cdot 10H_2O + Mg_2B_6O_{11} \cdot 15H_2O$
2	0.63	2.60	0.034	96.74	19.30	79.66	2963.73	1.02498	1.3389	$Na_2B_4O_7 \cdot 10H_2O + Mg_2B_6O_{11} \cdot 15H_2O$
3	1.05	2.48	0.035	96.44	29.45	69.57	2705.05	1.0275	1.3392	$Na_2B_4O_7 \cdot 10H_2O + Mg_2B_6O_{11} \cdot 15H_2O$
4	1.36	2.34	0.035	96.27	36.41	62.65	2577.38	1.0292	1.3398	$Na_2B_4O_7 \cdot 10H_2O + Mg_2B_6O_{11} \cdot 15H_2O$
5	1.58	2.22	0.035	96.17	41.20	57.89	2507.56	1.03173	1.3404	$Na_2B_4O_7 \cdot 10H_2O + Mg_2B_6O_{11} \cdot 15H_2O$
6	1.72	2.18	0.035	96.07	43.71	55.40	2441.30	1.03305	1.3407	$Na_2B_4O_7 \cdot 10H_2O + Mg_2B_6O_{11} \cdot 15H_2O$
7	2.01	2.12	0.036	95.83	48.25	50.89	2300.38	1.03486	1.3412	$Na_2B_4O_7 \cdot 10H_2O + Mg_2B_6O_{11} \cdot 15H_2O$
8	2.12	2.12	0.036	95.72	49.58	49.58	2238.63	1.03573	1.3413	$Na_2B_4O_7 \cdot 10H_2O + Mg_2B_6O_{11} \cdot 15H_2O$
9	2.29	2.11	0.037	95.56	51.61	47.55	2153.78	1.03868	1.3419	$Na_2B_4O_7 \cdot 10H_2O + Mg_2B_6O_{11} \cdot 15H_2O$
10	2.39	2.10	0.037	95.47	52.79	46.39	2108.97	1.04018	1.3425	$Na_2B_4O_7 \cdot 10H_2O + Mg_2B_6O_{11} \cdot 15H_2O$
11, E	3.40	2.07	0.044	94.49	61.66	37.54	1713.57	1.04909	1.3443	$Li_2B_4O_7 \cdot 3H_2O + Na_2B_4O_7 \cdot 10H_2O + Mg_2B_6O_{11} \cdot 15H_2O$
12, B	3.71	0.00	0.04	96.25	98.93	0.00	2566.67	1.03285	1.3424	$Li_2B_4O_7 \cdot 3H_2O + Mg_2B_6O_{11} \cdot 15H_2O$
13	3.68	0.78	0.041	95.50	81.76	17.33	2121.73	1.03901	1.3426	$Li_2B_4O_7 \cdot 3H_2O + Mg_2B_6O_{11} \cdot 15H_2O$
14	3.62	1.27	0.041	95.07	73.41	25.76	1927.99	1.04107	1.3427	$Li_2B_4O_7 \cdot 3H_2O + Mg_2B_6O_{11} \cdot 15H_2O$
15	3.6	1.47	0.042	94.89	70.42	28.76	1856.18	1.04177	1.3431	$Li_2B_4O_7 \cdot 3H_2O + Mg_2B_6O_{11} \cdot 15H_2O$
16	3.57	1.60	0.042	94.79	68.50	30.70	1818.65	1.04248	1.3433	$Li_2B_4O_7 \cdot 3H_2O + Mg_2B_6O_{11} \cdot 15H_2O$
17	3.45	1.85	0.043	94.66	64.57	34.62	1771.61	1.04533	1.3438	$Li_2B_4O_7 \cdot 3H_2O + Mg_2B_6O_{11} \cdot 15H_2O$
18, C	3.28	2.12	0.00	94.60	60.74	39.26	1751.85	1.04835	1.3441	$Li_2B_4O_7 \cdot 3H_2O + Na_2B_4O_7 \cdot 10H_2O$
19	3.34	2.10	0.022	94.54	61.15	38.45	1730.83	1.04871	1.3442	$Li_2B_4O_7 \cdot 3H_2O + Na_2B_4O_7 \cdot 10H_2O$

Point E stand for invariant point, which are saturated with ($Li_2B_4O_7 \cdot 3H_2O$ + $Na_2B_4O_7 \cdot 10H_2O$ + $Mg_2B_6O_{11} \cdot 15H_2O$ + Liquid), the compositions of $Li_2B_4O_7$, $Na_2B_4O_7$, $Mg_2B_6O_{11}$ in the liquid phase are 3.40, 2.07, and 0.044 in mass percentage (10^2 w), respectively. Due to the high solubilities of lithium borate and borax, there is a strong salting-out effect to magnesium borate.

Figure 2 is the water-phase diagram of the quaternary system at 298.15 K, and it shows that the Jänecke index values of $J(H_2O)$ gradually change with increasing of $J(Li_2B_4O_7)$.

The solid phase minerals were identified with X-ray diffractometer, hydrated salts including $Li_2B_4O_7 \cdot 3H_2O$, $Na_2B_4O_7 \cdot 10H_2O$, and $Mg_2B_6O_{11} \cdot 15H_2O$ existed in the system, and neither double salts nor solid solutions were found. Figure 3 shows the X-ray diffraction patterns of invariant point. The abscissa is the 2θ from 5° to 70°; the vertical ordinate is the intensity. The XRD pattern of the invariant point was well matched to standard diffraction pattern of $Li_2B_4O_7 \cdot 3H_2O$, $Na_2B_4O_7 \cdot 10H_2O$, and $Mg_2B_6O_{11} \cdot 15H_2O$ with powder diffraction file (pdf) number "43-1498", "33-1215", "36-0423", respectively. It shows that salts $Li_2B_4O_7 \cdot 3H_2O$, $Na_2B_4O_7 \cdot 10H_2O$, and $Mg_2B_6O_{11} \cdot 15H_2O$ coexist at the invariant point.

The Solution Physicochemical Properties of the Quaternary System

On the basis of experimental data in Table 1, relationship of the solution density and refractive index with the concentration of $Li_2B_4O_7$ in the quaternary system ($Li_2B_4O_7$ + $Na_2B_4O_7$ + $Mg_2B_6O_{11}$ + H_2O) at 298.15 K were plotted in Fig. 4. It was found that the solution density and refractive index in the quaternary system changed regularly with the increasing of $J(Li_2B_4O_7)$.

In Fig. 4a, the density curves of the equilibrium liquid phase increased gradually with the increasing of

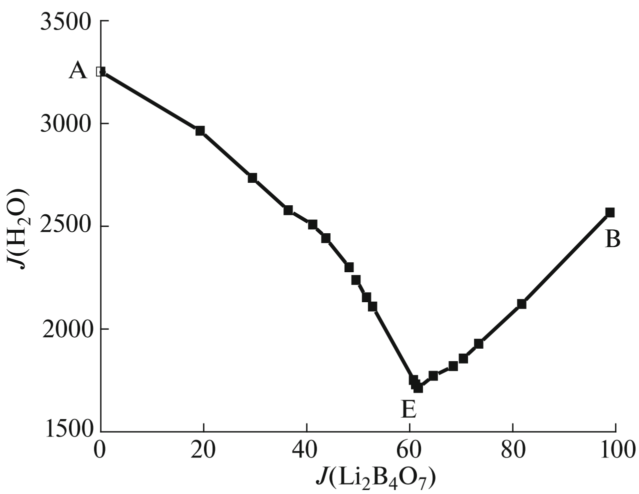

Fig. 2. Water-phase diagram of the quaternary system ($Li_2B_4O_7 + Na_2B_4O_7 + Mg_2B_6O_{11} + H_2O$) at 298.15 K.

$J(Li_2B_4O_7)$ (curves AE and CE), and reached the maximum value of 1.04909 g cm^{-3} at the invaraint point E, and then the solution densities was decreased sharply with the increasing concentration of $Li_2B_4O_7$ (curve EB).

Figure 4b shows the refractive index value versus composition of $Li_2B_4O_7$ in the solution. Similarly as the density in the solution, the refractive index value was increased slowly from point A to points E, while decreased sharply from point E to point B with the increasing of $J(Li_2B_4O_7)$, and the maximum value of 1.3443 at the invariant point of E.

Empirical Equations for Density and Refractive Index

Based on the following empirical equations of the density and refractive index in electrolyte solutions developed in the previous study [16], the density and refractive index of the solution were also calculated.

$$\ln\frac{\rho_t}{\rho_0} = \sum A_i w_i,\ \ln\frac{n_{Dt}}{n_{D0}} = \sum B_i w_i. \qquad (1)$$

In the above equations, where ρ_t and ρ_0 refer the density value of the solution and the pure water at the same temperature; the ρ_0 value of pure water at 298.15 K is 0.99704 g cm^{-3}. While n_{Dt} and n_{D0} refer the refractive index value of the solution and the pure water at the same temperature; the n_{D0} value of pure water at 298.15 K is 1.33250 [17]. A_i and B_i are the constants of each possible component i in the system, and they were calculated in the present work. w_i is the salt of i in the solution with weight percentage, in mass fraction. Constants A_i of $Li_2B_4O_7$, $Na_2B_4O_7$ and $Mg_2B_6O_{11}$ for calculation of density in solution are 0.000883, 0.009076, and 0.01092 at 298.15 K, and constants B_i of $Li_2B_4O_7$, $Na_2B_4O_7$, and $Mg_2B_6O_{11}$ for calculation of refractive index in solution are 0.00155, 0.00167, and 0.00938 at 298.15 K, respectively. All calculated results with the maximum relative error are less than 0.21%. The calculated values agree well with the experimental data, and this agreement shows that the coefficients A_i and B_i obtained in this work are reliable and can be used for more complicated systems containing borate.

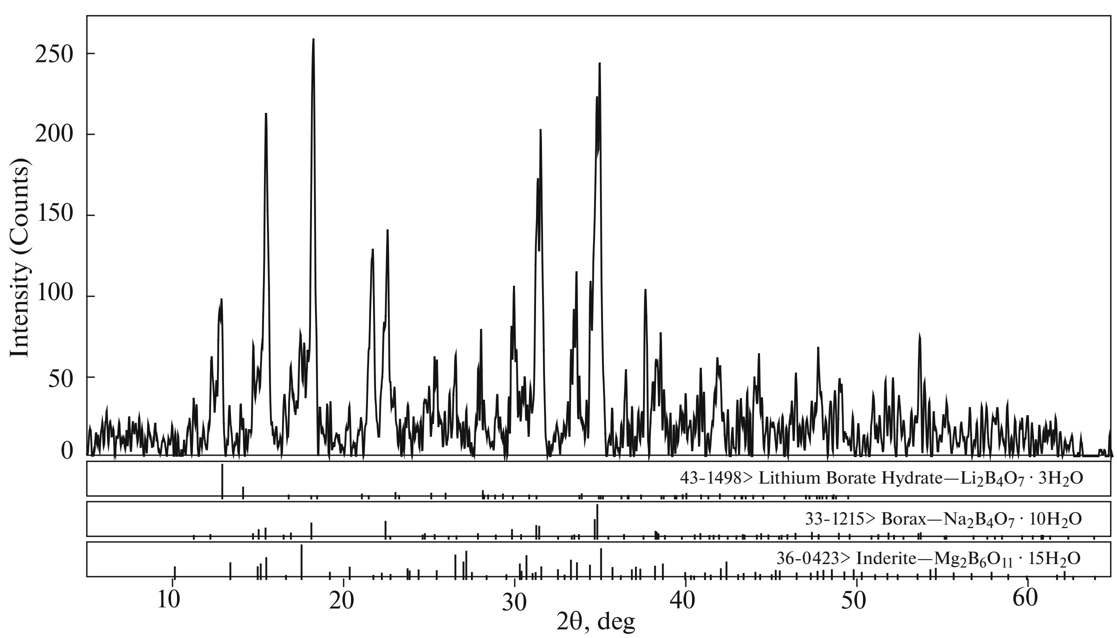

Fig. 3. X-ray diffraction pattern of the invariant point ($Li_2B_4O_7 \cdot 3H_2O + Na_2B_4O_7 \cdot 10H_2O + Mg_2B_6O_{11} \cdot 15H_2O$).

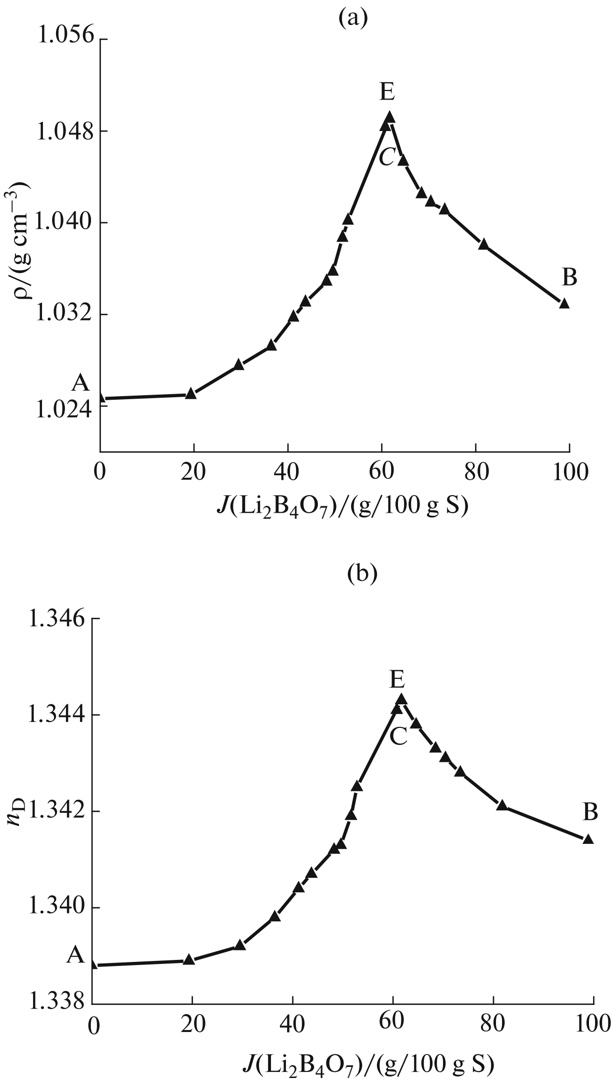

Fig. 4. Density and refractive index of the solution versus composition diagram of the quaternary system ($Li_2B_4O_7$ + $Na_2B_4O_7$ + $Mg_2B_6O_{11}$ + H_2O) at 298.15 K; (a) density versus composition (b) refractive index versus composition.

CONCLUSIONS

The solubilities, solution densities and refractive indices of the quaternary system ($Li_2B_4O_7$ + $Na_2B_4O_7$ + $Mg_2B_6O_{11}$ + H_2O) were determined using the isothermal dissolution method at 298.15 K, respectively. According to experimental data, the equilibrium phase diagrams and the diagrams of density and refractive index versus concentration of $Li_2B_4O_7$ were constructed. Phase diagram of the quaternary system consists of one invariant point ($Li_2B_4O_7 \cdot 3H_2O$ + $Na_2B_4O_7 \cdot 10H_2O$ + $Mg_2B_6O_{11} \cdot 15H_2O$ + Liquid) and three crystallization regions corresponding to $Li_2B_4O_7 \cdot 3H_2O$, $Na_2B_4O_7 \cdot 10H_2O$ and $Mg_2B_6O_{11} \cdot 15H_2O$. The size of crystallization areas of salts is in the order $Mg_2B_6O_{11} \cdot 15H_2O$ > $Na_2B_4O_7 \cdot 10H_2O$ > $Li_2B_4O_7 \cdot 3H_2O$. The solution density and refractive index in the quaternary system changed regularly with increasing of $Li_2B_4O_7$ concentration in the solution. The calculated values of density and refractive index using empirical equations for the quaternary system ($Li_2B_4O_7$ + $Na_2B_4O_7$ + MgB_4O_7 + H_2O) at 298.15 K are in good agreement with the experimental values.

ACKNOWLEDGMENTS

The work was supported by the Program of the National Natural Science Foundation of China (nos. U1507109, U1407113, 21406048, U1607123, 21773170, and 21106103), the Natural Science Foundation of Tianjin (no. 17JCYBJC19500), the Program for Changjiang Scholars and Innovative Research Team in University (IRT-17R81), the Innovative Research Team of Tianjin Municipal Education Commission (TD12-5004), and the Specialized Research Fund for Doctoral Program of Chinese Higher Education (no. 20111208120003) are greatly acknowledged.

REFERENCES

1. P.S. Song and Y. Yao, Calphad, **25**, 329 (2001).
2. X. Y. Zheng, M. G. Zhang, Y. Xu, et al., *Salt Lakes in China* (Chin. Sci., Beijing, 2002).
3. S. Y. Gao, P. S. Song, S. P. Xia, and M. P. Zheng, *Tibet Saline Lake Chemistry: A New Type of Boronm Lithium Salt Lake* (Chin. Sci., Beijing, 2007).
4. S. Q. Wang and T. L. Deng, J. Chem. Thermodyn. **40**, 1007 (2008).
5. D. L. Gao, Q. Wang, Y. F. Guo, et al., Fluid Phase Equilibr. **371**, 121 (2014).
6. S. Q. Wang, Y. F. Guo, J. S. Yang, et al., Russ. J. Phys. Chem. A **89**, 2190 (2015).
7. S. Q. Wang, Y. F. Guo, W. J. Liu, et al., J. Solution Chem. **44**, 1545 (2015).
8. T. L. Deng, S. Q. Wang, and B. Sun, J. Chem. Eng. Data **53**, 411 (2008).
9. D. C. Li, J. S. Yuan, and S. Q. Wang, Russ. J. Phys. Chem. A **88**, 42 (2014).
10. D. L. Gao, Y. F. Guo, X. P. Yu, et al., J. Chem. Eng. Data **60**, 2594 (2015).
11. F. Li, S. S. Zhang, Y. F. Guo, et al., Chin. SciPaper **9**, 1080 (2014).
12. S. Q. Wang, X. N. Han, Y. Jing, et al., J. Chem. Eng. Data **61**, 1155 (2016).
13. S. Q. Wang, Y. F. Guo, D. C. Li, et al., J. Chem. Eng. Data **60**, 821 (2015).
14. S. Q. Wang, F. Y. Guo, D. C. Li, et al., Thermochim. Acta **601**, 75 (2015).
15. J. Gao, Y. F. Guo, S. Q. Wang, et al., J. Chem. **2013**, 1 (2013).
16. C. H. Fang, J. Salt Lake Res. **2**, 15 (1990).
17. J. M. Speight, *Lange's Handbook of Chemistry*, 16th ed. (McGraw-Hill, New York, 2005).